THE UNIVERSITY OF
WARWICK

For more information, please contact the WRAP Team at: wrap@warwick.ac.uk
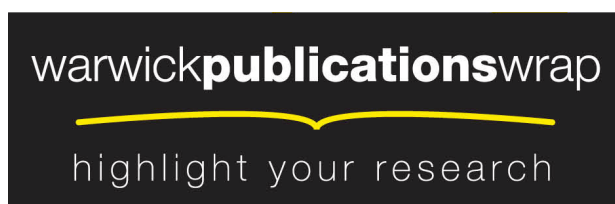
warwick**publications**wrap

highlight your research

http://go.warwick.ac.uk/lib-publications

Electrochemical Mapping Reveals Direct Correlation between Heterogeneous Electron Transfer Kinetics and Local Density of States in Diamond Electrodes**

Hollie V. Patten, Katherine E. Meadows, Laura A. Hutton, James G. Iacobini, Dario Battistel, Kim McKelvey, Alexander W. Colburn, Mark E. Newton, Julie V. Macpherson, Patrick R. Unwin**

Heterogeneous electron transfer (HET) processes at electrode/electrolyte interfaces are of widespread fundamental and applied importance, and are intensively studied by a wide range of techniques.[1] Even for nominally simple outer-sphere HET, the measured potential-dependent rate can depend on many factors[2] associated with the redox couple, the solvent and the electrode itself. In this regard, heterogeneous electrochemical processes are further complicated by the fact that the vast majority of electrode/electrolyte systems involve solid electrodes that have spatially non-uniform properties which may impact significantly on the local activity.

Polycrystalline boron doped diamond (pBDD) is a well-known heterogeneous electrode material, gaining increasing traction for a number of important applications.[3],[4] The different facets that make up the crystallites in pBDD contain different amounts of boron, resulting in a heterogeneously doped electrode surface. The material is generally considered metal-like for $[B] > 10^{20}$ cm^{-3} and semiconducting for $[B] < 10^{19}$ cm^{-3}, with a region between these limits characterized by hopping conduction.[5] Although different models have been proposed to describe HET at conducting polycrystalline pBDD electrodes,[6] there is uncertainty as to the most realistic model, as it has not yet been possible to determine how the local dopant density, and particularly the local density of states (LDOS) at the Fermi level, influences HET rates. Previous

attempts to extract HET kinetics at pBDD have used either cyclic voltammetry, which averages over large variations in surface properties[6],[7] or local techniques, such as scanning electrochemical microscopy (SECM)[6],[8] and electrogenerated-chemiluminescence microscopy.[9] Although significant heterogeneities in HET were observed by SECM,[6],[7b],[8b],[8c] the spatial resolution was insufficient to enable measurements to be related directly to local properties.

Focusing on outer sphere HET at metal-like pBDD, which is the material used most, the goal of this paper is to address key outstanding issues. We deliberately chose to work with oxygen-terminated surfaces as hydrogen-termination results in electrochemical unstable surfaces[10] and confers an additional level of complexity on elucidation of the HET process.[11] We show unequivocally, for the first time, that: (i) HET rates are directly linked to the local doping levels; (ii) there is no evidence of any enhancement of HET at grain boundaries; and (iii) HET rates correlate quantitatively with the LDOS in this heterogeneous material. These new insights are not only important in aiding the development of electrochemical technologies based on pBDD, but are also of considerable general value in identifying key factors that control HET at carbon-based electrodes.

The heterogeneous doping of a typical area of oxygen-terminated pBDD, used herein, can be seen clearly in Figure 1(a), which shows a field emission-scanning electron microscopy (FE-SEM) image of the surface of a polished pBDD electrode (roughness ~ 1 - 2 nm). Previous electron microscopy (EM) studies[12] have shown that secondary electron emission yields from pBDD reach a maximum at $[B]$ ca. 10^{19} cm^{-3}; thus, the darker areas in the image in Figure 1(a) typically represent zones which contain a higher amount of boron. This is confirmed by the Raman map of the same area, in Figure 1(b). The integrated peak area of the diamond zone center optical phonon (~ 1332 cm^{-1}) decreases with increasing boron content, as the peak shifts to lower wavenumbers. This indicates that the darker areas in Figure 1(b) represent regions of higher boron content.[8b, 13]

Individual Raman spectra were further analyzed in regions of the surface with the lowest and highest apparent boron levels, and across facets. Characteristic spectra for each of these regions (Supporting Information, section S1) display a clear, asymmetric diamond (sp^3) peak centered ca. 1332 cm^{-1}. It is worth noting that there is no evidence of peaks in the region 1350-1580 cm^{-1},[14] associated with sp^2 carbon, which may accumulate at grain boundaries. Asymmetry of the 1332 cm^{-1} peak, the so-called "Fano resonance", increases with increasing $[B]$[13] and is diagnostic of $[B] > 10^{20}$ atoms cm^{-3}.[8b, 13] The observation of the Fano resonance, in all Raman spectra, indicates that although the pBDD is heterogeneously doped, there are no semiconducting regions.

[*] H. V. Patten, K. E. Meadows, Dr. L. A. Hutton, J. G. Iacobini, K. McKelvey, Dr. A. W. Colburn, Prof. J. V. Macpherson, Prof. P. R. Unwin
Department of Chemistry, University of Warwick
Coventry, CV4 7AL (UK)
E-mail: p.r.unwin@warwick.ac.uk;
j.macpherson@warwick.ac.uk

K. E. Meadows, K. McKelvey
MOAC Doctoral Training Centre, University of Warwick
Coventry, CV4 7AL (UK)

D. Battistel
Department of Physical Chemistry, University of Venice
CalleLarga, S. Marta, 2137, 30123 Venice (Italy)

Dr. M. E. Newton
Department of Physics, University of Warwick
Coventry, CV5 7LL (UK)

Intermittent contact (IC)-SECM[15] was used in substrate generation-tip collection (SG-TC) mode[16] to map HET rates of the same region of the pBDD surface shown in Figure 1(a) and (b). The pBDD substrate was biased at a potential, E, of -0.170 V versus Ag/AgCl wire[17] reference electrode (RE), to reduce $Ru(NH_3)_6^{3+}$ from the bulk solution (5 mM in 50 mM KNO_3). This corresponded to an overpotential (η), $E - E^{o'} = -0.004$ V, where $E^{o'}$ is the formal potential determined from cyclic voltammetry (CV) recorded at the pBBD electrode in the same experiment. The tip (disk of radius, $a = 1.0$ µm; ratio of sheath to electrode radii,[18] RG=10) was held at 0.0 V. At this potential, $Ru(NH_3)_6^{2+}$ produced at the pBDD surface, diffuses toward the bulk of the solution and is collected by the tip. Pt wire served as a counter electrode in a 4-electrode set-up: see Supporting Information, section S2. IC-SECM was key to these measurements as it enabled the tip-substrate separation, d, to be maintained at a small and constant value of 1.0 µm for the entire image, so enhancing the dynamic (current) range and spatial resolution.[15] A clear and striking correlation can be seen between the boron dopant concentrations of individual facets (Figures 1(a,b)) and the corresponding tip currents in Figure 1(c). There is no evidence of enhanced activity at grain boundaries and no area of the surface is electrochemically inactive. Thus, the model for HET at metal-like pBDD is one where HET mirrors the doping of individual facets.

Finite element simulations (detailed in Supporting Information, section S3) were employed to determine the relationship between the tip current and standard HET rate constant, k^0, by applying Butler-Volmer kinetics at the pBDD surface. A transfer coefficient, $\alpha = 0.5$ was assumed, which is reasonable for outer sphere redox couples, especially as voltammetric analysis is relatively insensitive for the determination of α in the range 0.3 - 0.7, for the kinetic regime of interest.[19] This enabled maps of k^0 to be produced directly from current images, with a typical result shown in Figure 1(d). The high mass transport rates in SECM yielded local k^0 values with good precision.
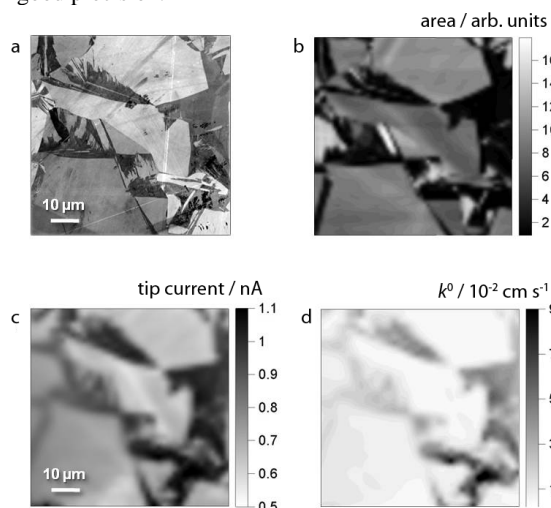

Figure 1. 70 µm × 70 µm images of pBDD obtained using (a) FE-SEM recorded with an in-lens detector at 2 kV; (b) Raman mapping, showing the integrated peak area at ~1332 cm-1 as a function of spot position; (c) IC-SECM SG-TC map for the collection of $Ru(NH_3)_6^{2+}$ (by oxidation), electrogenerated at the surface of pBDD (η = -0.004 V); and (d) k^0 values calculated from the currents in (c) using finite element simulations.

The electrochemical images highlight that, in the main, there are two distinct regions of HET activity, associated with the high and low boron-doped facets, as indicated in the Raman map (Figure 1(b)). To assign k^0 for these two regions, kinetic images were analyzed using a threshold method, as described in Supporting Information, section S4, giving $k^0 = 3.3$ (± 1.5) × 10^{-2} cm s-1 (high doped facets) and 0.7 (± 0.3) × 10^{-2} cm s-1 (low doped facets), respectively. Note that the $Ru(NH_3)_6^{3+/2+}$ data further reinforce the Raman observation that the pBDD surface contains no semiconducting regions, as the redox potential for $Ru(NH_3)_6^{3+/2+}$ lies in the band gap of semiconducting BDD,[8a],[6] for which significantly lower rates of HET, than recorded here, would have been expected.

To further elucidate HET rates at pBDD electrodes, the oxidation of ferrocenylmethyltrimethylammonium, $FcTMA^+$, was investigated. This reaction has proven useful for the investigation of electrode kinetics at other carbon-based electrodes[20] and $E^{o'}$ for $FcTMA^{2+/+}$ is considerably more positive, by 0.54 V, than for $Ru(NH_3)_6^{3+/2+}$. As for the data set reported in Figure 1, both FE-SEM and Raman images, Figures 2(a) and (b), respectively, were recorded in the same area as the IC-SECM image (Figure 2(c)) to allow direct correlation of electrochemical activity with doping levels. In this case, the bulk solution contained 1 mM $FcTMA^+$ (50 mM KNO_3) and a tip of $a = 1.3$ µm, at $d = 1.0$ µm was employed. The substrate was biased at a potential of +0.420 V versus Ag/AgCl wire (η = 0.045 V) to oxidize $FcTMA^+$, while the tip was biased at 0.0 V to collect any $FcTMA^{2+}$, generated at the pBDD substrate, at a diffusion-controlled rate. Distinct zones of tip current activity are again observed which correlate precisely with the areas of high and low dopant concentrations, evident in Figure 2(b). The corresponding k^0 map, shown in Figure 2(d), further highlights the contrasting electrochemical activity between different characteristic facets. Analysis to determine k^0 for the two differently doped regions (see Supporting Information, section S4) yielded 9.7 (± 4.0) × 10^{-2} cm s-1 (high doped) and 2.2 (± 0.8) × 10^{-2} cm s-1 (low doped). The data suggests that on both facet types (high and low doped), k^0 for $FcTMA^{2+/+}$ is approximately 3-fold higher than for $Ru(NH_3)_6^{3+/2+}$. This is qualitatively consistent with the higher self-exchange rate constant for ferrocenes.[21] Perhaps most interesting is that the ratio of the high to low k^0 values is similar (ca. 4) for each of the two different redox couples.
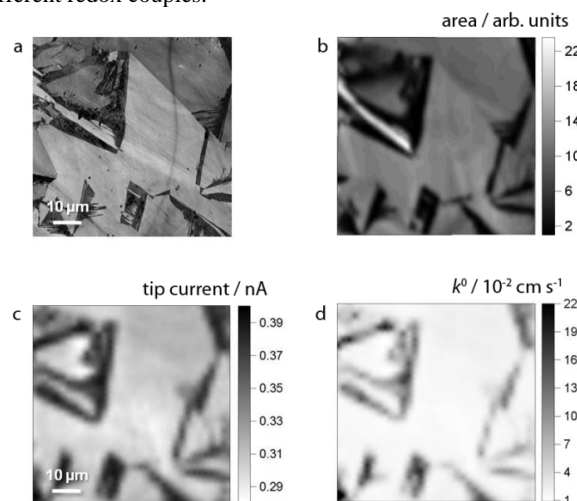
Figure 2. 70 µm × 70 µm images of pBDD obtained using (a) FE-SEM recorded with an in-lens detector at 2 kV, (b) Raman mapping, showing the integrated peak area at ~1332 cm-1 as a function of spot position; (c) IC-SECM SG-TC map for the collection of $FcTMA^{2+}$ (by reduction) electrogenerated at the surface of the pBDD (η = 0.045 V) and (d) calculated k^0 values from the currents in (c) using finite element simulations.

To explore the origins of this observation, we sought information on the LDOS of the two characteristic facets via local capacitance measurements. Measuring capacitance on the microscale by electrochemical methods is challenging due to the small signals that result, compared to those from sources of stray capacitance, which must be minimized. Although photolithographic techniques have recently been employed to prepare samples of graphene for the measurement of the quantum capacitance,[22] such an approach could not be implemented for the pBDD samples, due to the irregular spacing and geometry of the high and low doped facets. Thus, we chose to use scanning electrochemical cell microscopy (SECCM)[23] as a new, general approach for high spatial resolution capacitance measurements.
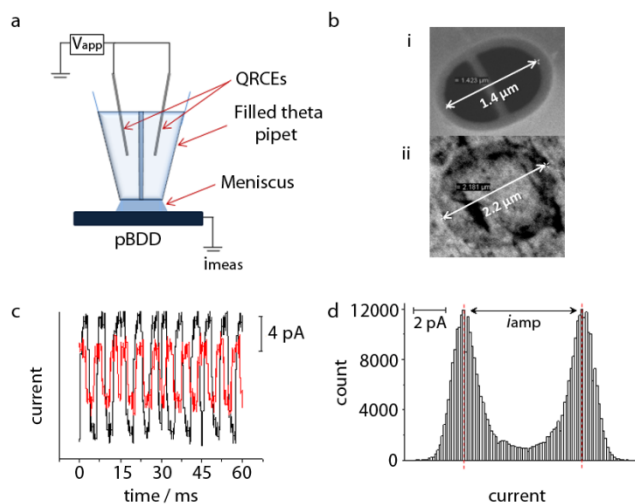

Figure 3. (a). Schematic of the SECCM set-up for recording capacitance on the micron-scale. (b) Typical FE-SEM images of (i) the end of a pulled theta capillary and (ii) residue remaining after the meniscus has been in contact with the substrate. (c) Typical capacitance current-time data in high (black) and low (red) doped regions of a pBDD substrate. (d) Histogram of the current amplitudes recorded during one typical measurement lasting ~ 45 s on a low doped facet.

A schematic of the SECCM set-up is shown in Figure 3(a). The probe consisted of a tapered theta glass capillary, drawn to a tip of size ~ 1.4 µm. Each chamber of the pipet, filled with electrolyte solution (50 mM KNO_3), contained a Ag/AgCl quasi-reference counter electrode (QRCE). For these measurements, an electrochemical cell was made when the meniscus at the end of the solution-filled capillary made contact with the pBDD substrate working electrode; grounded and under ambient conditions. Supporting Information, section S5 provides further details. Figure 3(b) shows typical FE-SEM images of: (i) a theta glass capillary end; and (ii) an imprint from the residue left on the pBDD surface from the meniscus contact, defining precisely the electrode area, A. Capacitance measurements were made over characteristic high and low doped regions of the surface, identified by optical microscopy in-situ with SECCM (with the high doped facets appearing darker). A 0.15 V peak-to-peak triangular wave centered on 0.0 V, scan rate, $v = 30$ V s^{-1}, was applied to the QRCEs with respect to the substrate working electrode (at ground). The corresponding square-wave current – time response, Figure 3(c), was diagnostic of the current flowing through a capacitance due to the potential wave-form applied[24] for the two differently-doped regions of the pBDD surface. It is evident that the different current amplitude, i_{amp}, in Figure 3(c) reflects the different doping levels of the facets. Figure

3(d) shows a typical histogram of the currents at the pBDD surface for one measurement (low doped facet) where the difference in the modal current values for the forward and reverse going potential scans define i_{amp}. The capacitance was extracted as $C_{meas} = i_{amp}/2vA$. Mean capacitance values were calculated to be 5.2 ± 0.8 µF cm^{-2} and 3.1 ± 0.4 µF cm^{-2} in the high and low doped regions, respectively. Note that the potential at which the measurements were made is in the mid-point region between the two redox couples. Over this potential region the capacitance of carbon electrodes varies only slightly[25] and we could not detect any differences in C_{meas} in this potential range within the precision of the microscale technique.

Even when pBDD diamond is doped sufficiently to be considered metal-like, C_{meas} has contributions from the Helmholtz capacitance, C_H, the diffuse layer capacitance, C_{diff}, and the capacitance of the space charge region, C_{SC} (eq. 1),[25b] due to the limited density of charge carriers compared to a typical metal. Thus, as for other carbon materials[25b, 25c],[26] we can write:

$$C_{meas}^{-1} = C_H^{-1} + C_{diff}^{-1} + C_{SC}^{-1} \qquad (1)$$

Under the high ionic strength conditions in these studies, $C_{diff} \gg C_H$ and so contributes negligibly in eq. 1.
C_{SC} is related to the LDOS at the Fermi level, $D(E_f)$ by:[25b, 27]

$$C_{SC} = \sqrt{e_o \varepsilon \varepsilon_o D(E_f)} \qquad (2)$$

where e_o is the electronic charge, ε is the dielectric constant of pBDD (5.5)[28] and ε_o is the vacuum permittivity. Assuming a typical value of $C_H \approx 20$ µF cm^{-2},[2c, 25b] the LDOS for the high and low boron doped facets is estimated as ~ 6.3 (± 2.0) $\times 10^{20}$ cm^{-3} eV^{-1} and ~ 1.7 (± 0.7) $\times 10^{20}$ cm^{-3} eV^{-1}, respectively, i.e. there is a difference of a factor of ~ 4 in the LDOS. For comparison metals have $D(E_f)$ ~ 10^{23} cm^{-3} eV^{-1}.[29]

The ratio of the LDOS in the high and low boron doped facets correlates with the ratio of k^0 values measured in these domains for the two different outer sphere redox couples. Thus, for this relatively highly doped oxygen-terminated carbon material, it is evident that the HET kinetics is governed to a large extent by the LDOS, which in turn is controlled by boron concentration. This produces a clear pattern of spatial HET activity in which rates are determined by the characteristics of particular facets and not by excess boron or sp^2 carbon accumulation at grain boundaries. This model of HET is of both fundamental value, and should also aid in the development and optimization of important emerging conducting diamond electrochemical technologies.

[1] a) D. E. Khoshtariya, T. D. Dolidze, M. Shushanyan, K. L. Davis, D. H. Waldeck, R. van Eldik, *Proc. Natl. Acad. Sci.* **2010**, *107*, 2757-2762; b) M. Shen, A. J. Bard, *J. Am.* Chem. *Soc.* **2011**, *133*, 15737-15742; c) J. F. Smalley, H. O. Finklea, C. E. D. Chidsey, M. R. Linford, S. E. Creager, J. P. Ferraris, K. Chalfant, T. Zawodzinsk, S. W. Feldberg, M. D. Newton, *J. Am. Chem. Soc.* **2003**, *125*, 2004-2013; d) R. W. Murray, *Chem. Rev.* **2008**, *108*, 2688-2720.
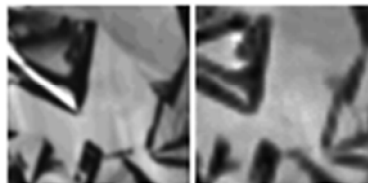
[2]   a) A. K. Mishra, D. H. Waldeck, *J. Phys. Chem C* **2009**, *113*, 17904-17914; b) K. Bano, A. Nafady, J. Zhang, A. M. Bond, H. Inam ul, *J. Phys. Chem C* **2011**, *115*, 24153-24163; c) A. J. Bard, L. R. Faulkner, *Electrochemical Methods: Fundamentals and Applications, 2nd Edition*, **2001**; d) S. Amemiya, N. Nioradze, P. Santhosh, M. J. Deible, *Anal. Chem.* **2011**, *83*, 5928-5935; e) S. Gosavi, R. A. Marcus, *J. Phys. Chem. B* **2000**, *104*, 2067-2072; f) J. Velmurugan, P. Sun, M. V. Mirkin, *J. Phys. Chem C* **2008**, *113*, 459-464; g) D. H. Evans, *Chem. Rev.* **2008**, *108*, 2113-2144; h) M. A. G. Zevenbergen, B. L. Wolfrum, E. D. Goluch, P. S. Singh, S. G. Lemay, *J. Am.* Chem. *Soc.* **2009**, *131*, 11471-11477.

[3]   J. Xu, M. C. Granger, Q. Chen, J. W. Strojek, T. E. Lister, G. M. Swain, *Anal. Chem.* **1997**, *69*, 591A-597A.

[4]   a) L. Hutton, M. E. Newton, P. R. Unwin, J. V. Macpherson, *Anal. Chem.* **2008**, *81*, 1023-1032; b) L. A. Hutton, M. E. Newton, P. R. Unwin, J. V. Macpherson, *Anal. Chem.* **2011**, *83*, 735-745; c) L. A. Hutton, M. Vidotti, J. G. Iacobini, C. Kelly, M. E. Newton, P. R. Unwin, J. V. Macpherson, *Anal. Chem.* **2011**, *83*, 5804-5808; d) T. Wu, G. Zhao, Y. Lei, P. Li, *J. Phys. Chem C* **2011**, *115*, 3888-3898; e) G. Zhao, P. Li, F. Nong, M. Li, J. Gao, D. Li, *J. Phys. Chem C* **2010**, *114*, 5906-5913; f) R. E. Ruther, M. L. Rigsby, J. B. Gerken, S. R. Hogendoorn, E. C. Landis, S. S. Stahl, R. J. Hamers, *J. Am. Chem. Soc.* **2011**, *133*, 5692-5694; g) A. Kirste, G. Schnakenburg, F. Stecker, A. Fischer, S. R. Waldvogel, *Angew. Chem. Int. Ed.* **2010**, *49*, 971-975; h) C. A. Martínez-Huitle, E. Brillas, *Angew. Chem. Int. Ed.* **2008**, *47*, 1998-2005.

[5]   J. P. Lagrange, A. Deneuville, E. Gheeraert, *Diamond Relat. Mater.* **1998**, *7*, 1390-1393.

[6]   K. B. Holt, A. J. Bard, Y. Show, G. M. Swain, *J. Phys. Chem. B* **2004**, *108*, 15117-15127.

[7]   a) M. C. Granger, M. Witek, J. Xu, J. Wang, M. Hupert, A. Hanks, M. D. Koppang, J. E. Butler, G. Lucazeau, M. Mermoux, J. W. Strojek, G. M. Swain, *Anal. Chem.* **2000**, *72*, 3793-3804; b) S. Haymond, G. T. Babcock, G. M. Swain, *Electroanalysis* **2003**, *15*, 249-253; c) D. Y. Kim, J. Wang, J. Yang, H. W. Kim, G. M. Swain, *J. Phys. Chem C* **2011**, *115*, 10026-10032.

[8]   a) A. Neufeld, A. O'Mullane, *J. Solid State Electrochem.* **2006**, *10*, 808-816; b) J. Chane-Tune, J.-P. Petit, S. Szunerits, P. Bouvier, D. Delabouglise, B. Marcus, M. Mermoux, *ChemPhysChem* **2006**, *7*, 89-93; c) N. R. Wilson, S. L. Clewes, M. E. Newton, P. R. Unwin, J. V. Macpherson, *J. Phys. Chem. B* **2006**, *110*, 5639-5646.

[9]   K. Honda, T. Noda, M. Yoshimura, K. Nakagawa, A. Fujishima, *J. Phys. Chem. B* **2004**, *108*, 16117-16127.

[10]   G. R. Salazar-Banda, L. S. Andrade, P. A. P. Nascente, P. S. Pizani, R. C. Rocha-Filho, L. A. Avaca, *Electrochim. Acta* **2006**, *51*, 4612-4619.

[11]   F. Maier, M. Riedel, B. Mantel, J. Ristein, L. Ley, *Phys. Rev. Lett.* **2000**, *85*, 3472-3475.

[12]   J. B. Miller, G. R. Brandes, *J. Appl. Phys.* **1997**, *82*, 4538-4545.

[13]   M. Bernard, A. Deneuville, P. Muret, *Diamond Relat. Mater.* **2004**, *13*, 282-286.

[14]   a) D. S. Knight, W. B. White, *J. Mater. Res.* **1989**, *4*, 385-393; b) P. K. Bachmann, D. Leers, H. Lydtin, *Diamond Relat. Mater.* **1991**, *1*, 1-12.

[15]   a) K. McKelvey, M. A. Edwards, P. R. Unwin, *Anal. Chem.* **2010**, *82*, 6334-6337; b) K. McKelvey, M. E. Snowden, M. Peruffo, P. R. Unwin, *Anal. Chem.* **2011**, *83*, 6447-6454.

[16]   a) R. D. Martin, P. R. Unwin, *Anal. Chem.* **1998**, *70*, 276-284; b) C. M. Sanchez-Sanchez, J. Rodriguez-Lopez, A. J. Bard, *Anal. Chem.* **2008**, *80*, 3254-3260; c) Y. Shen, M. Trauble, G. Wittstock, *Anal. Chem.* **2008**, *80*, 750-759.

[17]   C. G. Williams, M. A. Edwards, A. L. Colley, J. V. Macpherson, P. R. Unwin, *Anal. Chem.* **2009**, *81*, 2486-2495.

[18]   J. Kwak, A. J. Bard, *Anal. Chem.* **1989**, *61*, 1221-1227.

[19]   M. V. Mirkin, A. J. Bard, *Anal. Chem.* **1992**, *64*, 2293-2302.

[20]   a) P. V. Dudin, M. E. Snowden, J. V. Macpherson, P. R. Unwin, *ACS Nano* **2011**, *5*, 10017-10025; b) I. Dumitrescu, P. V. Dudin, J. P. Edgeworth, J. V. Macpherson, P. R. Unwin, *J. Phys. Chem C* **2010**, *114*, 2633-2639.

[21]   a) P. J. Smolenaers, J. K. Beattie, *Inorg. Chem.* **1986**, *25*, 2259-2262; b) G. M. Brown, N. Sutin, *J. Am. Chem. Soc.* **1979**, *101*, 883-892.

[22]   J. Xia, F. Chen, J. Li, N. Tao, *Nat Nano* **2009**, *4*, 505-509.

[23]   a) N. Ebejer, M. Schnippering, A. W. Colburn, M. A. Edwards, P. R. Unwin, *Anal. Chem.* **2010**, *82*, 9141-9145; b) S. C. S. Lai, P. V. Dudin, J. V. Macpherson, P. R. Unwin, *J. Am. Chem. Soc.* **2011**, *133*, 10744-10747; c) M. E. Snowden, A. G. Güell, S. C. S. Lai, K. McKelvey, N. Ebejer, M. A. O'Connell, A. W. Colburn, P. R. Unwin, *Anal. Chem.* **2012**, *84*, 2483-2491.

[24]   R. J. Rice, R. L. McCreery, *Anal. Chem.* **1989**, *61*, 1637-1641.

[25]   a) J. Xu, Q. Chen, G. M. *Swain*, *Anal. Chem.* **1998**, *70*, 3146-3154; b) H. Gerischer, *The Journal of Physical Chemistry* **1985**, *89*, 4249-4251; c) J. D. Wiggins-Camacho, K. J. Stevenson, *J. Phys. Chem C* **2009**, *113*, 19082-19090.

[26]   I. Heller, J. *Kong*, K. A. Williams, C. Dekker, S. G. Lemay, *J. Am. Chem. Soc.* **2006**, *128*, 7353-7359.

[27]   M. Hahn, M. Baertschi, O. Barbieri, J. C. Sauter, R. Kotz, R. *Gallay*, *Electrochem. Solid-State Lett.* **2004**, *7*, A33-A36.

[28]   C. E. Nebel, J. Ristein, in *Semiconductors and Semimetals, Vol. Volume 77* (Eds.: E. N. Christoph, R. Jürgen), Elsevier, **2004**, pp. xiii-xiv.

[29]   H. Gerischer, *Electrochim. Acta* **1990**, *35*, 1677-1699.

Hollie V. Patten, Katherine E. Meadows,
Laura A. Hutton, James G. Iacobini,
Dario Battistel, Kim McKelvey,
Alexander W. Colburn, Mark E. Newton,
Julie V. Macpherson*, Patrick R. Unwin*
_____ **Page – Page**

Dopant density   Kinetics

Electrochemical Mapping Reveals Direct
Correlation between Heterogeneous
Electron Transfer Kinetics and Local
Density of States in Diamond Electrodes

Using a multi-microscopy approach, we show for the first time that local heterogeneous electron transfer rates at conducting diamond electrodes correlate with the local density of electronic states. This new model of electroactivity is of considerable value for the rational design of conducting diamond electrochemical technologies, and also provides key general insights on electrode structure controls in electrochemical kinetics.